

Proceedings of the ASME 2021 Conference on Smart Materials,
Adaptive Structures and Intelligent Systems
SMASIS2021
September 14-15, 2021, Virtual, Online

## SMASIS2021-68200

# TRANSVERSE WAVE PROPAGATION BANDGAP IN A BUCKLED KIRIGAMI SHEET

Hesameddin Khosravi, and Suyi Li

Department of Mechanical Engineering, Clemson University Clemson, South Carolina, USA 29631

## **ABSTRACT**

This study examines the transverse elastic wave propagation bandgap in a buckled kirigami sheet. Kirigami — the ancient art of paper cutting — has become a design and fabrication framework for constructing metamaterials, robotics, and mechanical devices of vastly different sizes. For the first time, this study focuses on the wave propagation in a buckled kirigami sheet with uniformly distributed parallel cuts. When we apply an in-plane stretching force that exceeds a critical threshold, this kirigami sheet buckles and generates an out-of-plane, periodic deformation pattern that can change the propagation direction of passing waves. That is, waves entering the buckled Kirigami unit cells through its longitudinal direction can turn to the out-ofplane direction. As a result, the stretched kirigami sheet shows wave propagation band gaps in specific frequency ranges. This study formulates an analytical model to analyze the correlation between such propagation bandgap and the kirigami geometry. This model first simplifies the complex shape of buckled kirigami by introducing "virtual" folds and flat facets in between them. Then it incorporates the plane wave expansion method (PWE) to calculate the dispersion relationship, which shows that the periodic nature of the buckled kirigami sheet is sufficient to create Bragg scattering propagation bandgap. This study's results could open up new dynamic functionalities of kirigami as a versatile and multi-functional structural system.

**Keywords:** *Kirigami*; *Buckling*; *Bragg Bandgap*;

## 1 Introduction

Recently, there have been many efforts to develop smart structural systems by harnessing the rapid advancements in metamaterial research, particularly regarding their unique elastic wave propagation properties [1, 2]. Metamaterials – materials constructed with a carefully designed and typically periodic architecture – predominantly obtain their mechanical properties from its underlying architecture's geometry (or topology) rather than the constituent material properties. Such geometryproperty coupling can impart metamaterials with many "unnatural" behaviors, such as negative Poison's ratio [3, 4], negative bulk modulus and mass density [5, 6], negative transformation acoustics [7–9], and hyper-elastic cloaking [10, 11]. Moreover, the periodicity embedded in the metamaterial also creates acoustic and elastic wave propagation bandgaps for vibration isolation and mitigation [12-16], and the frequency range of such bandgap is controllable by directly tuning the underlying periodicity [17, 18].

To fully materialize the promising potentials of metamaterials, it is crucial to develop versatile, scalable, and easy-to-fabricate methods that can *both generate and tailor* the underlying periodic architecture [19, 20]. To this end, we propose the use of kirigami — a popular recreational art of cutting and manipulating paper — as a platform to create periodicity and wave propagation bandgaps. The Japanese word of kirigami means "cut"-"paper." It involves adding slit cuts to a flat sheet material and then transform it into a three-dimensional shape by stretching and folding [21]. The simplicity of kirigami has inspired many innovative engineering solutions for fabricating super-stretchable electronics [22,23], adaptive structures [24,25],

 $<sup>{}^*</sup>Address\ all\ correspondence\ to\ this\ author:\ hkhosra@clemson.edu$ 

and transformable robots [26, 27]. This study adopts a simple kirigami pattern involving a "zig-zag" distributed parallel slit cuts. If one stretches it beyond a critical load, it will buckle into a three-dimensional and periodic shape (Figure 1). By simply adjusting the post-buckling stretching force, one can control the shape of the kirigami and thus achieve structural adaptation.

This study aims to examine the wave propagation bandgap created by the stretch-buckled Kirigami sheet, particularly the transverse wave. We first propose a methodology to simplify the 3D geometry of post-buckled kirigami by introducing "virtual folds" and assuming flat facets in-between these folds. Then, we apply the plane wave expansion (PWE) method [28, 29] to the simplified kirigami geometry and calculate the dispersion relationships, showing the existence of a propagation bandgap. We conduct additional calculations to illustrate how the bandgap frequencies are directly related to kirigami designs, illustrating the versatility of this concept.

In the following part of this paper, section 2 details the geometry of the stretch-buckled kirigami sheet; section 3 summarizes the technical background, including wave propagation through periodic metamaterial, governing equations of motion, and plane wave expansion method; section 4 shows the theoretical predictions of wave propagation bandgaps with two different kirigami designs; and the last section 5 concludes this paper with a discussion.

## 2 Geometry of Stretch-Buckled Kirigami

Figure 1(a) explains the parameters defining the parallel and zig-zag distributed cutting pattern. Here,  $l_a$ ,  $l_b$ , and  $l_c$  define the slit cuts' lengths and the gap in-between two adjacent cuts; W is the spacing between two cuts along the longitudinal direction. Once buckled via stretching, the kirigami sheet takes a complicated three-dimensional shape with significant out-of-plane deformation. As a result, the buckled kirigami structure has a finite thickness, satisfying Euler-Bernoulli's beam geometrical conditions. In other words, the stretch-buckled Kirigami sheet becomes a beam-like structure consisting of a linear periodic array of "unit cells" as shown in Figure 1(c).

The ligaments inside the unit cells exhibit complex deformations with a non-uniform curvature distribution, making it challenging to calculate the parameters relevant to wave propagation analyses, such as the cross-sectional area and area moment of inertia. To address this challenge, we introduce "virtual folds" at critical locations on the ligaments that exhibit the most concentrated bending deformation and assume the facets in-between these folds are flat surfaces (Surfaces A, B, and C in Figure 1(d) and 2). Indeed, these folds can naturally occur when the stretching is strong enough to induce plastic deformation [30], so they could represent the mechanics of buckled kirigami sheets with reasonable accuracy. Moreover, the simplified kirigami becomes

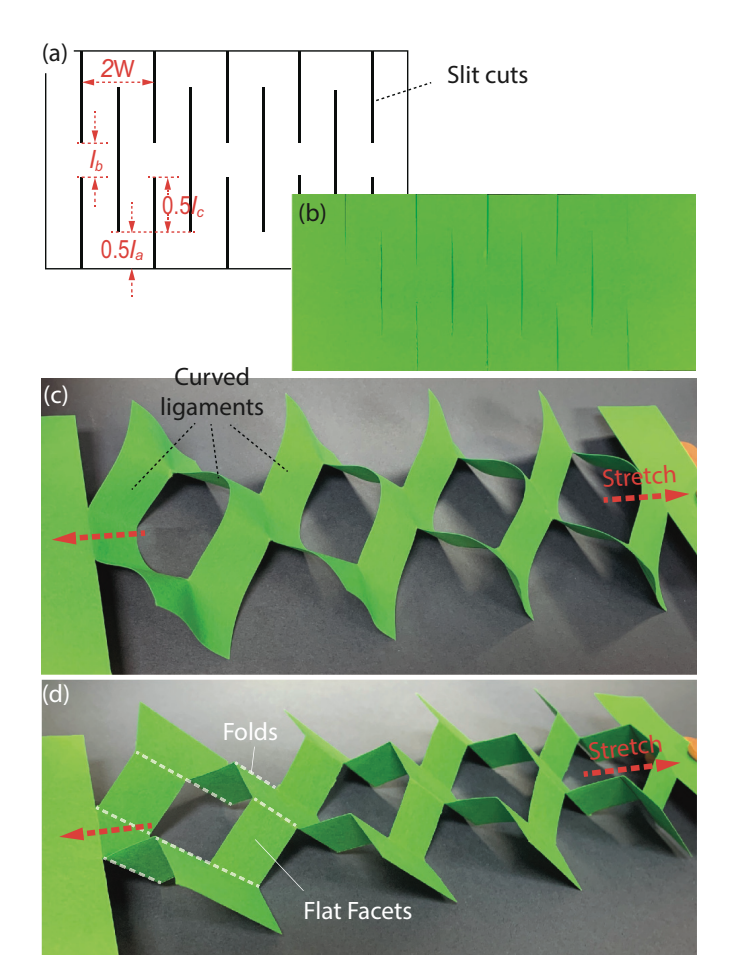


FIGURE 1: The geometry of the stretch-buckled kirigami sheet.

(a) Schematic of the kirigami cutting pattern consisting of "zigzag" distributed parallel cuts. (b) A paper-based prototype before stretching. (c) The original stretch buckled kirigami sheet, showing a complex out-of-plane deformation and curved "ligaments." (d) The stretched kirigami sheet with a simplified geometry, where the buckling-induced deformations are concentrated to the folds so that the surfaces in-between the folds remain flat.

rigid-foldable, making the kirigami deformation a one degree-of-freedom mechanism.

To solve the dynamic equation of motion for wave propagation (as we detail later in Section 3), we need to calculate the distribution of cross-sectional area A(x) and bending moment of inertia I(x) over a unit cell, where x represents the longitudinal direction. To this end, we choose the dihedral angle  $(\varphi)$  between the Surface B within the kirigami unit cell and the y-z reference plane as the independent variable (Figure 2(c)). When the kirigami sheet is un-deformed (or flat in the x-y reference plane),  $\varphi$  takes the maximum value  $(\varphi_{max} = \pi/2)$ ; when the buckled kirigami sheet is fully stretched,  $\varphi$  take the minimum

value:

$$\varphi_{\min} = \tan^{-1} \left( \frac{2W}{l_c} \right). \tag{1}$$

We also denote the dihedral angle between Surface C defined in Figure 2 and the x - z reference place as  $\beta$ , so that

$$\beta = \cos^{-1}\left(\frac{2W}{l_c \tan \varphi}\right). \tag{2}$$

 $\beta=\pi/2$  when the Kirigami sheet is un-deformed (flat), and  $\beta=0$  when the Kirigami sheet is fully stretched. The overall length of the unit cell is

$$a = \frac{2W}{\sin \varphi}. (3)$$

Another important geometric variable is the *projected* length of Surface C along the y axis as illustrated in Figure 2(b):

$$d = W \frac{\tan \beta}{\tan \varphi} = \sqrt{\frac{l_c^2}{4} - \frac{W^2}{\tan^2 \varphi}} = \frac{l_c}{2} \sin \beta. \tag{4}$$

Here, we assume the kirigami sheet is highly stretched after buckling in that  $\phi_{min} < \varphi < \pi/4$  (assuming  $l_c > 2W$ ). We can divide half of the unit cell in this case into three sections (Section i, ii, and iii in Figure 2(c)) because the cross-sections take distinct shapes in these three sections (Figure 2(c)).

The first Section i corresponds to  $0 < x < W \sin \phi$ , and the cross-sectional areas involves surface B and surface C. The cross section (solid lines in Figure 2(b<sub>i</sub>)) is the summation of these two parts so that

$$A_{i}(x) = \frac{t}{\sin \varphi} \left( l_{b} + 2L_{i}^{C} \right)$$

$$= \frac{t}{\sin \varphi} \left( l_{b} + \frac{x}{W \sin \varphi} \sqrt{4W^{2} + l_{c}^{2} \tan^{4} \varphi} \right),$$
(5)

where t is the thickness of the kirigami sheet material. The bending moment of inertia with respect to the y-axis also includes two parts:

$$I_{i}(x) = I^{B} + l_{b} \frac{t}{\sin \varphi} \left(\frac{x}{\tan \varphi}\right)^{2} + 2I_{i}^{C} + \dots$$

$$2\frac{x \tan \beta}{\cos \varphi} \frac{t}{\sin \varphi} \left(\frac{x \tan \varphi - x \cot \varphi}{2}\right)^{2},$$
(6)

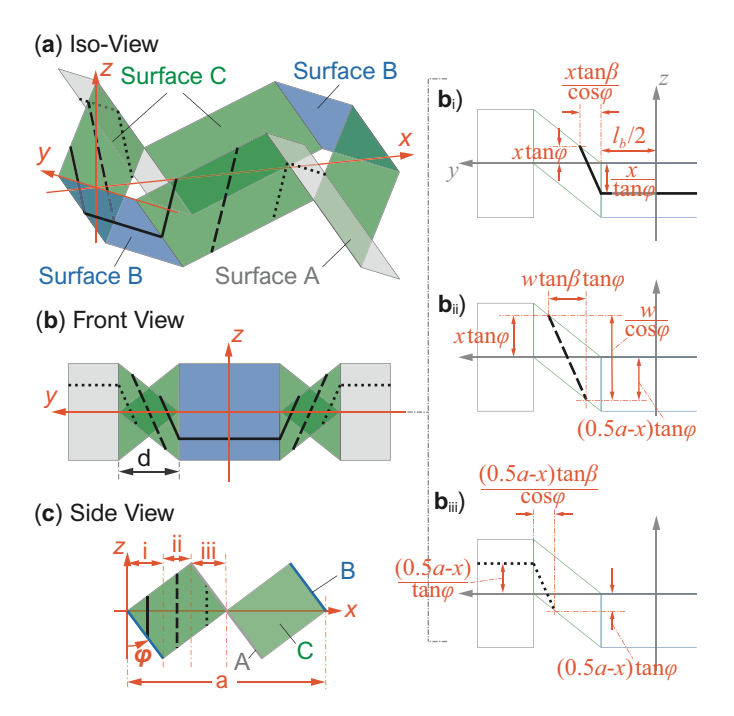


**FIGURE 2**: The unit cell geometry of a simplified Kirigami sheet with a relatively large stretch. (a-c): The isometric, front, and side view of Kirigami unit cell, respectively. Notice that the independent variable  $\varphi$  and the three sections in the half unit cells are highlighted in the side view. ( $b_i$ - $b_{iii}$ ): Close-up front view of the cross-section area corresponding to different x values. Notice that the solid, dashed, dotted black lines are the cross-section of the kirigami unit cell in three different sections.

where the first two terms come from the cross-section of Surface B (using parallel axis theorem), and the third and fourth terms come from the cross-section of Surface C. Here,  $I^B$  is the bending moment of inertia of the Surface B's cross-section with respect to its own neutral axis in that

$$I^{B} = \frac{l_{b}}{12} \left( \frac{t}{\sin \varphi} \right)^{3}. \tag{7}$$

Similarly,  $I_i^C$  is Surface C's bending moment of inertia with respect to its own neutral axis in that

$$I_i^C(x) = \frac{t}{12\sin\varphi} \frac{x\tan\beta}{\cos\varphi} \left[ \frac{t^2}{\sin^2\varphi} + x^2(\tan\varphi + \cot\varphi)^2 \right]$$
(8)

The second Section ii corresponds to  $w \sin < x < a/2 - w \sin \varphi$ , and the overall cross-section area involves Surface C (dashed line in Figure 2(b<sub>ii</sub>)).

$$A_{ii}(x) = 2\frac{t}{\sin \varphi} L_{ii}^{C} = \frac{t}{\sin \varphi} \sqrt{4W^2 + l_c^2 \tan^4 \varphi}.$$
 (9)

The bending moment of inertia with respect to the y-axis is

$$I_{ii}(x) = 2I_{ii}^{C} + 2\frac{t}{\sin \varphi} \left[ (a/4 - x) \tan \varphi \right]^{2},$$
 (10)

where

$$I_{ii}^{C} = \frac{t}{12\sin\varphi}W\tan\varphi\tan\beta\left(\frac{t^{2}}{\sin^{2}\varphi} + \frac{W^{2}}{\cos^{2}\varphi}\right).$$
 (11)

Finally, the third Section iii of the half unit cell corresponds to  $\sin \varphi < x < a/2$ . In this section, the cross-section (dotted line in Figure 2(b<sub>iii</sub>)) involve Surface A and C in that

$$A_{iii}(x) = \frac{t}{\sin \varphi} \left( l_a + 2L_{iii}^C \right)$$

$$= \frac{t}{\sin \varphi} \left( l_a + \frac{a/2 - x}{W \sin \varphi} \sqrt{4W^2 + l_c^2 \tan^4 \varphi} \right).$$
(12)

The corresponding bending moment of inertia with respect to the y-axis includes two components in that,

$$I_{iii}(x) = I^A + l_a \frac{t}{\sin \varphi} \left( \frac{a/2 - x}{\tan \varphi} \right)^2 + 2I_{iii}^C + \dots$$

$$2 \frac{(a/2 - x) \tan \beta}{\cos \varphi} \frac{t}{\sin \varphi} \left[ \frac{(a/2 - x)(\tan \varphi - \cot \varphi)}{2} \right]^2, \tag{13}$$

where,

$$I_{iii}^{C}(x) = \frac{t}{12\sin\varphi} \frac{(a/2 - x)\tan\beta}{\cos\varphi} \dots$$

$$\left[\frac{t^2}{\sin^2\varphi} + (a/2 - x)^2(\tan\varphi + \cot\varphi)^2\right],$$
(14)

and  $I^A$  is the bending moment of inertia of the cross-section area in Surface A with respect to its own neutral axis so that

$$I^{A} = \frac{l_a}{12} \left( \frac{t}{\sin \varphi} \right)^3. \tag{15}$$

## 3 Wave Propagation Bandgap Analysis

This section details the wave propagation and bandgap analysis in the stretch-buckled kirigami sheet using the plane wave expansion (PWE) method. First, we introduce the equations of motions governing the elastic wave propagation in the beam-like,

buckled kirigami structure. Then, we expand these equations over the periodic unit cells by Blotch's theory. Finally, by applying the geometry parameters obtained in Section 2, we formulate an analytical solution describing the dispersion relationship and bandgap frequencies in the stretched kirigami.

**Governing Equation of Motion** Here, we apply free-free boundary conditions to the stretch-buckled kirigami and only allow transverse waves (in the z-direction) to propagate along the x-direction. Suppose the buckled kirigami's overall thickness in the z direction and width in the y direction are significantly smaller than the length in the x direction, we can describe it as an Euler-Bernoulli beam — by neglecting the shearing deformation and rotational inertia of the cross-sections — based on the governing equation:

$$\frac{\partial^2}{\partial x^2} \left[ E(x) I(x) \frac{\partial^2 U(x,t)}{\partial x^2} \right] + \rho(x) A(x) \frac{\partial^2 U(x,t)}{\partial t^2} = 0, \quad (16)$$

where  $\rho(x)$  and E(x) are the mass density and Young's modulus distribution, respectively. They are constant in this case since we assume the kirigami sheet is made of homogeneous sheet material. U(x,t) is the transverse displacement field in the out-of-plane z direction. The cross-section area A(x) and the second moment of inertia I(x) have been calculated in Section 2

**Lattice Vectors** Here we briefly review some fundamental concepts regarding periodic structures. A two-dimensional periodic structure can be represented by a set of infinite translation operations on a unit cell along specific directions, and the corresponding translational vectors are:

$$\mathbf{V} = a_1 \mathbf{e}_1 + a_2 \mathbf{e}_2. \tag{17}$$

In this equation,  $\mathbf{e}_1$  and  $\mathbf{e}_2$  are called the lattice vectors in the direct space, and  $a_1$  and  $a_2$  are integers. The translational vector's dimension depends on the nature of periodicity, and its direction defines the orientations of the underlying periodicity.

The reciprocal lattice is defined as the set of vectors **G** that satisfy the following relationship  $e^{-i\mathbf{G}\cdot\mathbf{V}}=1$ , where  $\mathbf{G}=m_1\mathbf{b}_1+m_2\mathbf{b}_2$ . Here,  $\mathbf{b}_1$  and  $\mathbf{b}_2$  are the lattice vectors in the reciprocal space. Simplification of the above relations leads to the conclusion that the reciprocal lattice vectors  $(\mathbf{b}_1, \mathbf{b}_2)$  are orthogonal to the original lattice vectors  $(\mathbf{e}_1, \mathbf{e}_2)$  in that

$$\mathbf{e}_i \cdot \mathbf{b}_i = 2\pi \delta_{ii} \tag{18}$$

Like the lattice vectors  $\mathbf{e}_1$ ,  $\mathbf{e}_2$  that define the periodicity in the direct space, reciprocal lattice vectors  $\mathbf{b}_1$ ,  $\mathbf{b}_2$  describe the corresponding periodicity in the reciprocal space. Moreover, based

on the connection between the direct and reciprocal lattice vectors, a "primitive" unit cell can be defined in the reciprocal space corresponding to the original unit cell, and such primitive unit cells are referred to as the first Brillouin zone [13]. The importance of the Brillouin zone stems from the Bloch description of the wave field in periodic media. It is found that the solutions to wave governing equations can be completely characterized by Bloch wave theory in the first Brillouin zone as multiplication of plane waves and a periodic function.

**Plane Wave Expansion Method (PWE)** Here, we apply the PWE method to the wave propagation problem and calculate the band structure induced by kirigami's periodicity. The band structures provide an abundance of information on the wave propagation characteristics.

The first step in implementing the PWE method is to apply the separation of variables to extract time as one independent variable from the displacement field  $U(\mathbf{r},t)$  in that

$$U(\mathbf{r},t) = \tilde{U}(\mathbf{r})e^{-i\omega t} \tag{19}$$

where  $\omega$  is the frequency of harmonic oscillation. Next, the spatial domain function  $\tilde{U}(\mathbf{r})$  are factorized as a combination of plane wave fields and harmonic function in the first Brillouin zone by Blotch theory,

$$\tilde{U}(\mathbf{r}) = e^{i\mathbf{K}\cdot\mathbf{r}} \sum_{\mathbf{H}} \hat{U}(\mathbf{H}) e^{i\mathbf{H}\cdot\mathbf{r}}.$$
 (20)

Now that  $\hat{U}(\mathbf{H})$  is a harmonic function in space. Here,  $\mathbf{H} = n_1\mathbf{b}_1 + n_2\mathbf{b}_2$  is a direction vector, where  $n_1$ ,  $n_2$  are integers.  $\mathbf{K} = k_1\mathbf{b}_1 + k_2\mathbf{b}_2$  is the wave vector, whose component can restricted to vary within the First Brillouin Zone in that  $k_1, k_2 \in [0, \frac{1}{2}]$ . We use the basis functions in the Fourier series expansion to represent the periodic geometrical properties and define the wave field as a set of all transverse wave numbers. These functions are expanded through the multiplication of reciprocal lattice vector  $\mathbf{G}$  with an increasing integer  $m_1$  and  $m_2$ . Therefore, the periodicity of geometrical parameters can be represented as:

$$I(\mathbf{r}) = \sum_{\mathbf{G}} \hat{I}(\mathbf{G}) e^{i\mathbf{G}\cdot\mathbf{r}}$$

$$A(\mathbf{r}) = \sum_{\mathbf{G}} \hat{A}(\mathbf{G}) e^{i\mathbf{G}\cdot\mathbf{r}}$$
(21)

Substituting the above terms in equations (19)-(21) into the equation (16), for a two-dimension case, we can re-rearrange the

equation of motion as:

$$\sum_{\mathbf{G}} \sum_{\mathbf{H}} \left[ E(\mathbf{H} + \mathbf{K})^{2} (\mathbf{K} + \mathbf{H} + \mathbf{G})^{2} \hat{I}(\mathbf{G}) - \omega^{2} \rho \hat{A}(\mathbf{G}) \right] \hat{U}(\mathbf{H}) e^{i(\mathbf{K} + \mathbf{G} + \mathbf{H}) \cdot \mathbf{r}} = 0$$
(22)

By defining a new vector  $\mathbf{G}'$ , such that  $\mathbf{G}' = \mathbf{G} + \mathbf{H}$ , we can shift the vector  $\mathbf{G}$  by  $\mathbf{H}$ . In addition, we eliminate the part  $\hat{U}(\mathbf{H})e^{i(\mathbf{K}+\mathbf{G}')\cdot\mathbf{r}}$  as it cannot take the zero value. Then, we obtain the characteristic equation in that

$$\sum_{\mathbf{G}'} \sum_{\mathbf{H}} \left[ E(\mathbf{H} + \mathbf{K})^2 (\mathbf{K} + \mathbf{G}')^2 \hat{I} (\mathbf{G}' - \mathbf{H}) - \omega^2 \rho \hat{A} (\mathbf{G}' - \mathbf{H}) \right] = 0.$$
(23)

Applications to Stretched Kirigami The stretchbuckled kirigami sheet is periodic only in the x direction (both stretched and unstretched). Therefore, we consider it a beam-like structure, and the position vector  $\mathbf{r}$  is one-dimensional, aligning with the x direction. For an observer at any location on the stretch-buckled kirigami, the structure appears to be an assembly of identical unit cells. If the kirigami is infinitely long and translated by any vector joining two cuts of the same type, it appears identical as it did before the translation. Therefore, the direct lattice vector and corresponding reciprocal lattice vectors are also one-dimensional and in x direction ( $V = a_1 e_1$ , and  $\mathbf{G} = m_1 \mathbf{b}_1$ ). Subsequently, the wave vector  $\mathbf{K} = k_1 \mathbf{b}_1$  and harmonic wave propagation  $\mathbf{H} = n_1 \mathbf{b}_1$ . Kirigami geometric properties — including the cross-section area A(x) and area moment of inertia I(x) — are periodic functions defined in the x direction through a unit cell. We expand these functions according to Equation 21. Finally, the dispersion curve with respect to changing wave number between [0, 0.5] is derived, and the results are discussed in the following section.

#### 4 Bandgap Structure Results

We apply the theoretical formulation from Section 3 to two stretched kirigami sheets with different cutting patterns. These two sheets have the same overall width  $L=l_a+l_b+l_c=0.122\mathrm{m}$ , spacing between cuts  $W=0.01\mathrm{m}$ , and sheet thickness  $t=0.002\mathrm{m}$ . Both kirigami sheets are assumed to be made of Nylon material so that  $E=9.2\mathrm{GPa}$  and  $\rho=1200\mathrm{kg/m^3}$ . However, they have different cut lengths. For the first sheet,  $l_a=0.04\mathrm{m}$ ,  $l_b=0.02\mathrm{m}$ , and  $l_c=0.062\mathrm{m}$ ; for the second sheet,  $l_a=0.05\mathrm{m}$ ,  $l_b=0.02\mathrm{m}$ , and  $l_c=0.052\mathrm{m}$ .

Figures 3 and 4 show the dispersion relationship of this kirigami sheet after buckling (solved using MATLAB). The first sheet is stretched until  $\varphi=27^{\circ}$ , while the second one is stretched until  $\varphi=32^{\circ}$ . The dispersion relationship clearly indicates the

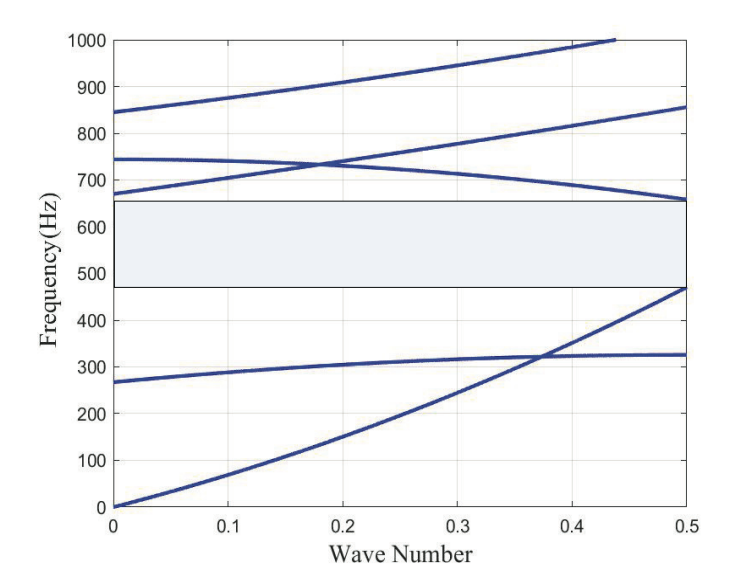


**FIGURE 3**: Band diagram for a stretched buckled kirigami by changing integer  $m_1 \in [-3,3]$ . bandgap in light blue for case 1.

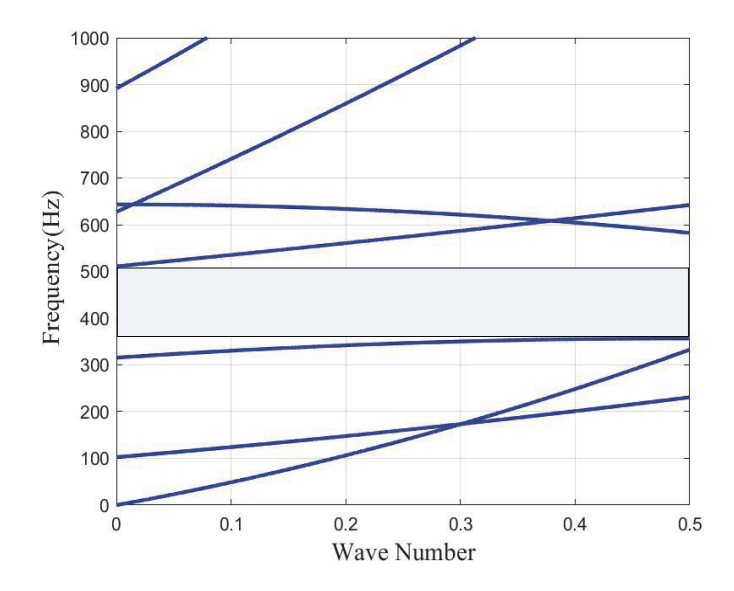


**FIGURE 4**: Band diagram for a stretched buckled kirigami by changing integer  $m_1 \in [-3,3]$ . bandgap in light blue for case 2.

existence of wave propagation bandgaps. For the first kirigami sheet, its bandgap occurs between 465 and 668Hz; and the second sheet shows a bandgap between 361 and 518Hz. Such differences in bandgap frequencies indicate that adjusting the cutting pattern of the kirigami sheet (and thus cross-sectional area A(x) and bending moment of inertia I(x) in the unit cell) is a simple

yet effective method to tailor the wave propagation behaviors.

## 5 Summary and Conclusion

This study examines the transverse wave propagation bandgaps in stretch-buckled Kirigami sheets. We conduct an analytical investigation using the plane wave expansion (PWE) method and the Bloch analysis on the unit cell of the kirigami sheet. The most significant challenges here come from the complicated 3D geometry of the unit cell, especially the curved ligaments. To this end, we propose a method to simplify the kirigami unit cell geometry by placing folds at the locations with the most concentrated deformation and then assuming flat facets inbetween these folds. Such simplification provides us with clear insight into the correlation between periodicity and cutting design in the stretched Kirigami sheet. It also makes the mathematical formulation manageable. We present the dispersion relationship and propagation bandgaps of two stretched kirigami sheets with different cut sizes. The results show that the bandgap properties can be tailored effectively through optimizing the underlying kirigami cuts pattern design. This study's results could open up new dynamic functionalities of kirigami as a versatile and multi-functional structural system.

## **ACKNOWLEDGMENT**

The authors acknowledge the support from National Science Foundation (CMMI-1760943). S Li also acknowledge the support from Clemson University CECAS Dean's Faculty Fellowship.

#### **REFERENCES**

- [1] Nouh, M. A., Aldraihem, O. J., and Baz, A., 2016. "Periodic metamaterial plates with smart tunable local resonators". *Journal of Intelligent Material Systems and Structures*, 27(13), pp. 1829–1845.
- [2] Zhu, Z. W., and Deng, Z. C., 2016. "Elastic wave propagation in adaptive honeycomb-based materials with high connectivity". *Smart Materials and Structures*, **25**(8).
- [3] Schenk, M., and Guest, S. D., 2013. "Geometry of Miura-folded metamaterials". *Proceedings of the National Academy of Sciences of the United States of America*, 110(9), pp. 3276–3281.
- [4] Chen, Y., Li, T., Scarpa, F., and Wang, L., 2017. "Lattice Metamaterials with Mechanically Tunable Poisson's Ratio for Vibration Control". *Physical Review Applied*, 7(2), pp. 1–11.
- [5] Ding, Y., Liu, Z., Qiu, C., and Shi, J., 2007. "Metamaterial with simultaneously negative bulk modulus and mass density". *Physical Review Letters*, *99*(9), pp. 2–5.

- [6] Liu, X. N., Hu, G. K., Huang, G. L., and Sun, C. T., 2011. "An elastic metamaterial with simultaneously negative mass density and bulk modulus". *Applied Physics Letters*, **98**(25), pp. 96–99.
- [7] Park, C. M., and Lee, S. H., 2019. "Zero-reflection acoustic metamaterial with a negative refractive index". *Scientific Reports*, **9**(1), pp. 1–7.
- [8] Haberman, M. R., and Guild, M. D., 2016. "Acoustic metamaterials". *Physics Today*, **69**(6), pp. 42–48.
- [9] Cummer, S. A., Christensen, J., and Alù, A., 2016. "Controlling sound with acoustic metamaterials". *Nature Reviews Materials*, 1(16001).
- [10] Parnell, W. J., and Shearer, T., 2013. "Antiplane elastic wave cloaking using metamaterials, homogenization and hyperelasticity". *Wave Motion*, *50*(7), pp. 1140–1152.
- [11] Xin, F., and Lu, T. J., 2017. "Self-controlled wave propagation in hyperelastic media". *Scientific Reports*, 7(1), pp. 1–9.
- [12] Trainiti, G., Rimoli, J. J., and Ruzzene, M., 2015. "Wave propagation in periodically undulated beams and plates". *International Journal of Solids and Structures*, **75-76**, pp. 260–276.
- [13] Thota, M., Li, S., and Wang, K. W., 2017. "Lattice reconfiguration and phononic band-gap adaptation via origami folding". *Physical Review B*, **95**(6), pp. 1–10.
- [14] Junyi, L., Ruffini, V., and Balint, D., 2016. "Measuring the band structures of periodic beams using the wave superposition method". *Journal of Sound and Vibration*, 382, pp. 158–178.
- [15] Wang, Y. F., Wang, Y. S., and Zhang, C., 2014. "Bandgaps and directional propagation of elastic waves in 2D square zigzag lattice structures". *Journal of Physics D: Applied Physics*, 47(48).
- [16] Wang, Y. Z., Li, F. M., Kishimoto, K., Wang, Y. S., and Huang, W. H., 2009. "Elastic wave band gaps in magnetoelectroelastic phononic crystals". *Wave Motion*, 46(1), pp. 47–56.
- [17] Ning, S., Yang, F., Luo, C., Liu, Z., and Zhuang, Z., 2020. "Low-frequency tunable locally resonant band gaps in acoustic metamaterials through large deformation". *Extreme Mechanics Letters*, *35*, p. 100623.
- [18] Wang, Y.-F., Wang, Y.-Z., Wu, B., Chen, W., and Wang, Y.-S., 2020. "Tunable and Active Phononic Crystals and Metamaterials". Applied Mechanics Reviews, 72(4).
- [19] Coulais, C., Sabbadini, A., Vink, F., and van Hecke, M., 2018. "Multi-step self-guided pathways for shape-changing metamaterials". *Nature*, *561*(7724), pp. 512–515.
- [20] Mirzaali, M. J., Janbaz, S., Strano, M., Vergani, L., and Zadpoor, A. A., 2018. "Shape-matching soft mechanical metamaterials". *Scientific Reports*, 8(1), pp. 1–7.
- [21] Rafsanjani, A., and Bertoldi, K., 2017. "Buckling-Induced Kirigami". *Physical Review Letters*, *118*(8), pp. 1–5.

- [22] Mortazavi, B., Lherbier, A., Fan, Z., Harju, A., Rabczuk, T., and Charlier, J. C., 2017. "Thermal and electronic transport characteristics of highly stretchable graphene kirigami". *Nanoscale*, *9*(42), pp. 16329–16341.
- [23] Wu, C., Wang, X., Lin, L., Guo, H., and Wang, Z. L., 2016. "Paper-Based Triboelectric Nanogenerators Made of Stretchable Interlocking Kirigami Patterns". *ACS Nano*, *10*(4), pp. 4652–4659.
- [24] Sun, J., Scarpa, F., Liu, Y., and Leng, J., 2016. "Morphing thickness in airfoils using pneumatic flexible tubes and Kirigami honeycomb". *Journal of Intelligent Material Systems and Structures*, **27**(6), pp. 755–763.
- [25] Chen, Y., Scarpa, F., Remillat, C., Farrow, I., Liu, Y., and Leng, J., 2014. "Curved Kirigami SILICOMB cellular structures with zero Poisson's ratio for large deformations and morphing". *Journal of Intelligent Material Systems and Structures*, 25(6), pp. 731–743.
- [26] Liu, B., Ozkan-Aydin, Y., Goldman, D. I., and Hammond, F. L., 2019. "Kirigami skin improves soft earthworm robot anchoring and locomotion under cohesive soil". *Ro-boSoft 2019 - 2019 IEEE International Conference on Soft Robotics*, pp. 828–833.
- [27] Tang, Y., Lin, G., Yang, S., Yi, Y. K., Kamien, R. D., and Yin, J., 2017. "Programmable Kiri-Kirigami Metamaterials". *Advanced Materials*, *29*(10), pp. 1–9.
- [28] De Miranda, E. J. P., and Dos Santos, J. M. C., 2017. "Flexural wave band gaps in phononic crystal euler-bernoulli beams using wave finite element and plane wave expansion methods". *Materials Research*, 20, pp. 729–742.
- [29] Shi, S., Chen, C., and Prather, D. W., 2004. "With Perfectly Matched Layers". *America*, *21*(9), pp. 1769–1775.
- [30] Isobe, M., and Okumura, K., 2016. "Initial rigid response and softening transition of highly stretchable kirigami sheet materials". *Scientific Reports*, **6**, apr, p. 24758.